Ceramics International 49 (2023) 23765–23774

Contents lists available at ScienceDirect

Ceramics International

journal homepage: www.elsevier.com/locate/ceramint

Incorporation and corrosion protection mechanism of TiO_2 nano-particles in SnAgCu composite alloys: Experimental and density functional theory study

Balázs Illés [a,b,*], Halim Choi [a], Jaeduk Byun [c], Karel Dušek [d], David Bušek [d], Agata Skwarek [b,e]

[a] Budapest University of Technology and Economics, Faculty of Electrical Engineering and Informatics, Department of Electronics Technology, Budapest, Hungary
[b] Łukasiewicz Research Network - Institute of Microelectronics and Photonics, LTCC Technology Research Group, Kraków, Poland
[c] Dankook University, Department of Physics, Cheonan, Republic of Korea
[d] Department of Electrotechnology, Faculty of Electrical Engineering, Czech Technical University in Prague, Prague, Czech Republic
[e] Gdynia Maritime University, Department of Marine Electronics, Gdynia, Poland

ARTICLE INFO

Handling Editor: Dr P. Vincenzini

Keywords:
Composite solder alloy
TiO_2 nano-particles
Corrosion protection
Sn whisker
Density functional theory
Grain refinement

ABSTRACT

This work studied the incorporation mechanism of TiO_2 nano-particles into SnAgCu solders and their effect on the corrosion behavior of the composite alloy. Composite solder alloys have been made from 99Sn0.3Ag0.7Cu solder alloy and TiO_2 nano-particles between 0.25 and 1 wt%. The alloys in solder joints were exposed to 4000 h long 85 °C/85RH% thermal-humidity test, and their surface was observed by SEM and FIB techniques. Large localized corrosion spots and numerous Sn whiskers have been found on the samples, except for the samples with 0.25 wt% TiO_2 content. The corrosion of the Sn grains resulted in a volumetric increase and mechanical stress, which was relaxed via whisker growth. TiO_2 nano-particles in 0.25 wt% incorporated layer-like at the boundaries of the Sn grain. Density functional theory calculations proved that at soldering conditions, the Sn atoms of the solder alloy could bond to the TiO_2 NPs through the O atoms of TiO_2. The TiO_2–Sn oxide layer at the grain boundaries could suppress the corrosion of the composite solder alloys and whisker growth. In the case of higher weight fractions TiO_2, the nano-particles were agglomerated and could not perform corrosion protection effect.

1. Introduction

Modern electronic devices are an essential part of our everyday life (industry, transportation, telecommunication, health care, etc.), and they are mostly produced by some kind of soldering technology. The introduction of Pb-free soldering resulted in the widespread application of different solder alloys [1]. The mostly applied are the high silver (Ag) content 95.5Sn4Ag0.5Cu (SAC405), 96.5Sn3Ag0.5Cu (SAC305), and the modern low Ag content SAC105 (98.5Sn1Ag0.5Cu), SAC0307 (99Sn0.3Ag0.7Cu). Krammer et al., 2015 reported, that the main problems with Ag are its continuously increasing price, and with higher Ag content in the solder alloy, the risk of thermo-mechanical problems like shrinkage defects increase [2]. However, the lower Ag content results in higher Sn content in the solder alloys, which might cause reliability problems, like the appearance of Sn whiskers [3]. Sn whiskers can grow on solder joints or surface finishes made from high Sn content alloys. Their length can reach even a millimeter, but typically, it is between 20 and 100 μm. Therefore, the Sn whiskers can cause a considerable reliability risk in the finer and finer microelectronics since they can establish short circuits between the component leads. The Sn whisker growth is the result of mechanical stress acting on the Sn object close to its surface [4].

Recently, solder alloys have been improved by adding ceramic reinforcement particles into them, resulting in a composite solder alloy. Usually, nano-particles (NPs), and sometimes nano-fibers (NFs) are used in 0.05 – 2 wt% weight fraction. Different materials, mostly oxide ceramics, have been successfully tested: Al_2O_3, SiC, TiO_2, ZrO_2, ZnO, Fe_2O_3, Si_3Ni_4, etc. [5–9]. The ceramic NPs are not soluble in the solders, so they incorporate at the Sn and intermetallic (Cu_6Sn_5, Cu_3Sn, and Ag_3Sn) grain boundaries [10,11], where they promote the heterogeneous nucleation [5]. This results in the suppression of grain growth (at all phases) and decreases dislocation motions [12,13]. The finer Sn and

* Corresponding author. Budapest University of Technology and Economics, Faculty of Electrical Engineering and Informatics, Department of Electronics Technology, Budapest, Hungary.
E-mail address: illes.balazs@vik.bme.hu (B. Illés).

https://doi.org/10.1016/j.ceramint.2023.04.216
Received 3 March 2023; Received in revised form 24 April 2023; Accepted 26 April 2023
Available online 26 April 2023

intermetallic (IMC) grains generally result in the imporovment of mechanical properties of the composite solder joints, like hardening of the Sn matrix [14], increases the tensile [10], yield strength [15,16], microhardness [10], and decrease the CTE [17]. The only known negative effect of the ceramic NPs is a minor increase in the liquidus temperature [18].

TiO_2 is the most frequently and most successfully applied reinforcement material in soldering technology. Tsao and Chang [10] investigated the thermal and microstructural parameters of Sn3.5Ag0.25Cu solder alloy with 0.25–1 wt% TiO_2 NPs. They reported 3.5–5.9 °C liquidus temperature increase and decrease of β-Sn, Ag_3Sn IMCs grains, and reduction of Ag_3Sn spacing, which resulted in an improvement in microhardness. Later they reported similar results in the case of Sn3.5Ag and Sn3.5Ag0.7Cu solder alloys [19]. The observed increase in the shear strength was explained by the classical dispersion strengthening theory and the decreased Cu_6Sn_5 IMC layer. Tang et al. [20] also studied the influence of TiO_2 NPs (between 0.05 and 0.6 wt%) on the thermal properties and wettability of SAC305 solder alloy. 4.4 °C increase in the liquidus temperature and decreased wetting angle (means better wetting) were observed. They found a decrease in the size of Ag_3Sn IMC grains and in their spacing, which resulted in 37% microhardness improvement [21].

Ani et al. [7] investigated Sn3.5Ag0.7Cu solder alloy with TiO_2 NPs between 0.05 and 0.15 wt%. TiO_2 NPs improved the fillet height, suppressed the IMC growth, and improved the wetting ability. Similar results were found by Ramili et al. [17] with the rare Sn0.7Cu0.05Ni solder alloy. Nasir et al. [22] observed 26% improvement in the hardness of Sn3.0Ag0.5Cu alloy after the addition of 1.0 wt % TiO_2 NPs. They also explained the hardening by the refined IMC structure in the solder joints. Skwarek et al. [23] reinforced SAC0307 solder alloy with TiO_2 NPs in 1 wt% amount and used it for soldering power LEDs. They found that TiO_2 NPs caused the thermal resistance decrease of the assembled LED by 20%, and they increased the luminous efficiency of the LEDs.

It can be concluded that the TiO_2 NPs seem to be very promising from the quality aspect of the composite solder alloys. However, the exact incorporation mechanism of TiO_2 NPs into the Sn-matrix is still not known. Furthermore, the effect of their refined microstructure on the reliability of the composite solder joints and layers has not been widely investigated. Therefore, our aims in this study were to describe the incorporation mechanism of TiO_2 NPs into the Sn-matrix and to investigate the effect of TiO_2 NPs' weight fraction on the corrosion resistance of the composite solder joints.

2. Materials and methods

TiO_2 rutile nano-particles of Sigma-Aldrich (primary particle size 21 nm) were used to reinforce the low Ag content SAC0307 (99Sn0.3Ag0.7Cu) solder paste of Alpha Industries. TiO_2 is usually applied between 0.1–1wt% [17,21], so the following three weight fractions were used: 0.25, 0.5, and 1 wt%. The NPs were mixed homogeneously into the solder paste by a YX solder paste mixing machine with 400 rpm for 10 min. Altogether, four solder compositions were used: SAC0307–0.25TiO_2, SAC0307-0.5TiO_2, SAC0307-1TiO_2, and pure SAC0307 as reference.

The solder alloys were investigated in the form of classical solder joints of surface-mounted chip resistors. Printed circuit boards (PCBs) were made from 1.6 mm thick FR4 glass fiber-epoxy composite laminate. The boards were covered with Cu foil (35 μm) on which solder pads were formed by wet chemical etching. The solder pads were covered by immersion Ag as surface finishing. A 125 μm thick stencil foil was used for the uniform deposition of solder pastes. Chip resistor (0603:1.5 × 0.75 mm sized with Cu/Ni contact cap) was placed into the solder deposits by pick and place method. An infrared (IR) reflow oven was applied to melt the solder paste and form the solder joints. A linear thermal profile was used: preheating phase (20–150 °C; 0–100s), soak phase (150–200 °C; 100–280s), ramp-up phase (200–250 °C; 280–350s).

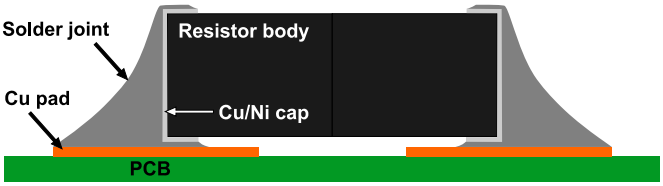

Fig. 1. Cross-sectional schematic of the assembled chip resistor.

Fig. 1 shows the cross-sectional schematic of the assembled chip resistor. The test boards with solder joints were exposed to a 4000 h long thermal-humidity (TH) test set to 85 °C/85RH%.

The surface of the solder joints was observed by a SEM device (FEI Inspect S50, using a thermal emission gun) every 500 h. For the microstructural studies, surface cuts and lamellae were prepared on the solder joints by a FIB device (Thermo Scientific Scios 2) and mechanical cross-sectioning. The microstructure of the solder joints was investigated by a finer FE-SEM device (Thermo Scientific Scios 2, using non-immersion field emission gun) and a STEM device (JEOL JEM-2100, using LaB6 gun). The elemental composition of the samples was investigated by EDS of the SEM and STEM devices. The interaction between the TiO_2 and the Sn atoms was studied by density functional theory (DFT) calculations using plane-wave/pseudopotential formalism. The calculations were carried out in the Quantum ESPRESSO software using the Perdew-Burke-Ernzerhof exchange-correlation functional.

3. Results

Fig. 2 shows the changes on the solder joints' surfaces in the case of a ref. SAC0307 and a SAC0307–0.25TiO_2 samples during the TH test. The observed solder joint was always the same in a given case. Fig. 2a and b were done after 1000 h TH test; however, they show the initial state of the observed solder joints since no deviation has been found yet. In Fig. 2b some flux residues can be seen on the solder joint (black spots), which is typical during reflow soldering. Furthermore, another typical soldering phenomenon is visible in the middle of both the solder joints (Fig. 2a and b), namely extensive Cu_6Sn_5 IMC networks, which means that the dispersed IMC pikes from solder bulk reached the surface.

Dark gray spots started to spread on the ref. SAC0307 sample after 1000 h (Fig. 2c), and were continuously growing during the TH test (Fig. 2e and g). Contrast differences of SEM-BSE micrograph indicate an elemental difference, which EDS results also proved later (see Fig. 4). The dark gray spots contained a considerably higher amount of O than the surroundings, so it meant that they were corrosion spots. Sn has two types of oxides: SnO or SnO_2, they were marked by SnO_x in the article. In the case of SAC0307–0.25TiO_2 samples, only minor corrosion spots were found (examples are barely visible in Fig. 2d, f, and h).

After 1500 h, not only corrosion spots but Sn whisker also appeared on the ref. SAC0307 solder joints (not on the observed one in Fig. 2). They usually grew next or in the corrosion spot (Fig. 2e and g). They were mostly twisted nodule type [24], and their typical length was 4–40 μm. It was reported earlier that the high Sn content SnAgCu solder alloys are prone to whiskers growth in corrosive conditions due to their lower corrosion resistance [24,25]. As the TH test approached, with the expansion of the corroded areas, more and more Sn whiskers appeared on the ref. SAC0307 samples (Fig. 2g). At the end of the investigations (after 4000 h), the upper meniscus of reference solder joints were almost continuously corroded and grew numerous whiskers (Fig. 2g). In the case of the SAC0307–0.25TiO_2 samples (Fig. 2b, d, f, and h), accordingly to the fact that the corrosion spots were very limited, only a very few short whiskers were found at the end of the investigations (they were not on the presented solder joint in Fig. 2).

Fig. 3 presents the surface changes of SAC0307-0.5TiO_2 and SAC0307-1TiO_2 samples during the 85C/85RH% TH test. The observed solder joint was always the same in a given case. Fig. 3a and b were done

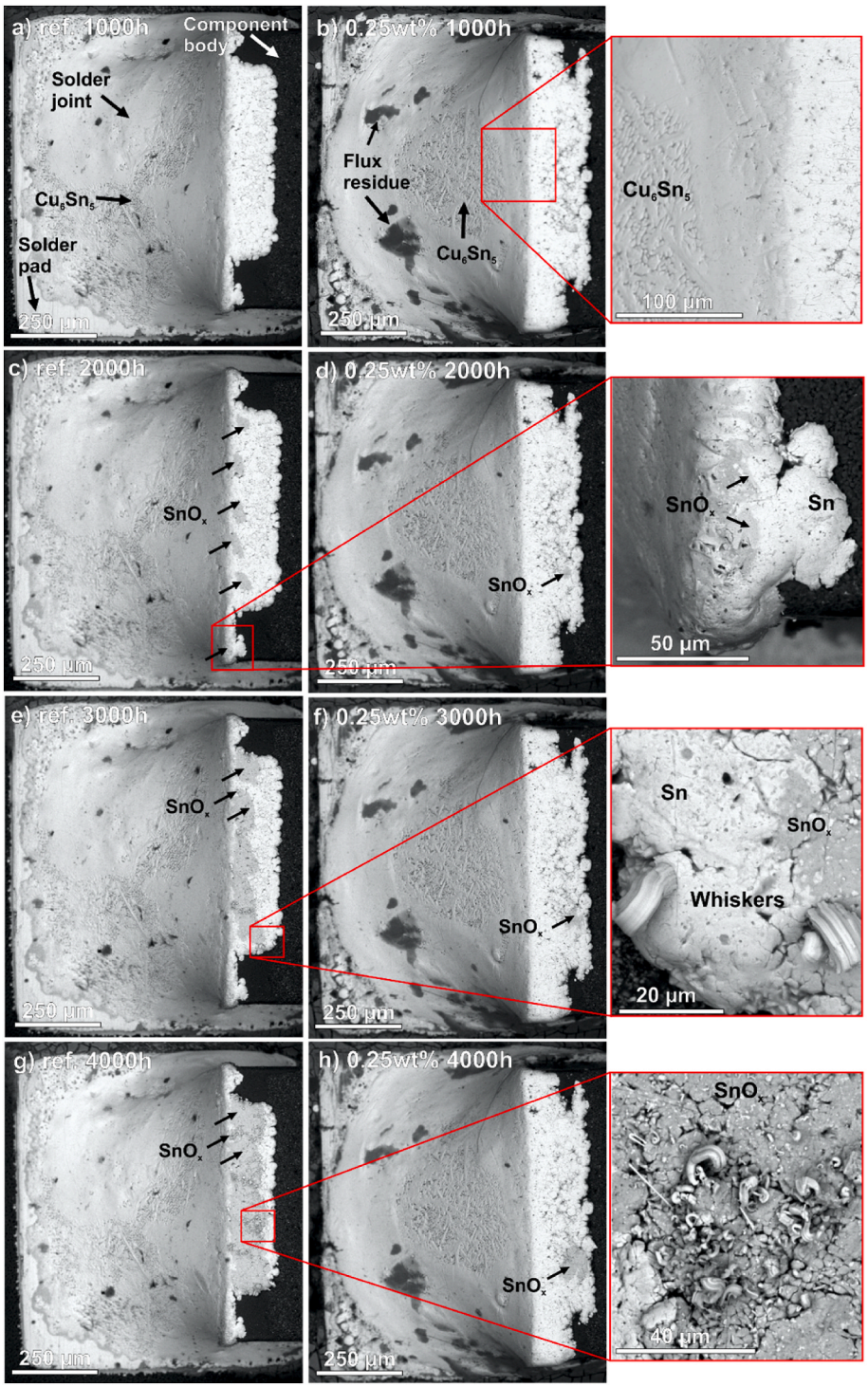

Fig. 2. SEM-BSE micrograph of a ref. SAC0307 and SAC-0.25TiO_2 solder joints during the 85C/85RH% TH test: a) ref. SAC0307 1000 h; b) SAC-0.25TiO_2 1000 h; c) ref. SAC0307 2000h; d) SAC-0.25TiO_2 2000h; e) ref. SAC0307 3000 h; f) SAC-0.25TiO_2 3000 h; g) ref. SAC0307 4000 h; h) SAC-0.25TiO_2 4000 h.

after 1000 h TH test; however, they show the initial state of the observed solder joints since no deviation has been found yet. The flux residues and the extensive Cu_6Sn_5 IMC networks were also observable in these joints too (Fig. 3a and b). Oppositely to the SAC0307–0.25TiO_2 solder joints, the SnO_x corrosion spots appeared on the solder joints with higher TiO_2 weight fractions after 1000 h of TH test (Fig. 3c and d). With the surface corrosion, the Sn whiskers also appeared on the SAC0307-0.5TiO_2 and SAC0307-1TiO_2 solder joints; firstly, they were detected at 1500 h. Fig. 3c and d presents typical examples of the detected nodule-type Sn whiskers. On these samples too, the whiskers usually grew next to the corroded areas, as it is well observable in Fig. 3e and f. The solder joints with higher TiO_2 content (0.5 and 1 wt%) behaved very similarly to the reference SAC0307 solder joint; namely, the corroded areas were continuously growing on them, as well as the number of Sn whiskers (Fig. 3e–h).

According to Figs. 2 and 3, it could seem that mostly the upper meniscus of the solder joints was corroded and produced whiskers, but it was not a fact. Fig. 4a shows an example that the corrosion and the

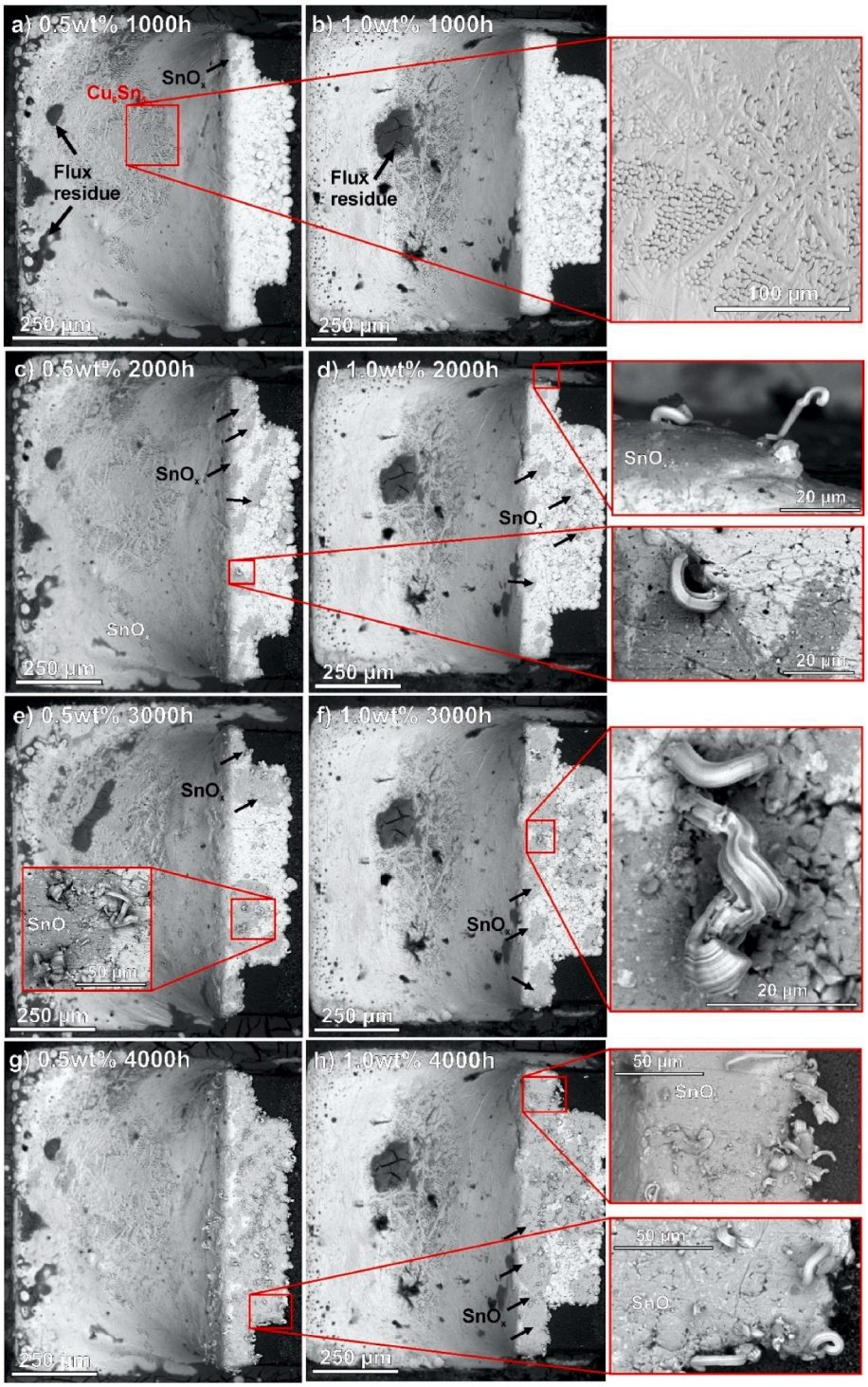

Fig. 3. SEM-BSE micrograph SAC-0.5TiO_2 and SAC-1TiO_2 solder joints during the 85C/85RH% TH test: a) SAC-0.5TiO_2 1000 h; b) SAC-1TiO_2 1000 h; c) SAC-0.5TiO_2 2000h; d) SAC-1TiO_2 2000h; e) SAC-0.5TiO_2 3000 h; f) SAC-1TiO_2 3000 h; g) SAC-0.5TiO_2 4000 h; h) SAC-1TiO_2 4000 h.

whisker growth were not limited to the upper meniscus (lower right corner of Fig. 3g in higher magnification). The marks of SnO_x and Sn whiskers are visible on the lower meniscus as well. Fig. 4b presents the EDS results (the end of the spectra were cut over 5 keV due to the visualisation), which prove that the dark gray areas on the surface of the solder joints were corroded (Fig. 4, M2 measurement point) since they contained remarkably more oxygen than the light gray areas (Fig. 4, M1 measurement point) in the SEM-BSE micrograph. The more intensive corrosion and whisker growth at the upper meniscus (horizontal part of the solder joints) could be caused by the better keeping of adsorbed/condensed water there than the inclined part of the meniscus of the solder joints.

The number of the detected Sn whiskers was counted on ten solder joints (Fig. 5). In the case of ref. SAC0307 and higher TiO_2 content (0.5 and 1 wt%) alloys, the number increase of the whiskers had exponential growth. More than 500 pcs. of Sn whiskers per 1 mm^2 were found on these samples till the end of the TH test (4000 h). The average length of the developed nodule whiskers was only between 10 and 20 µm. The

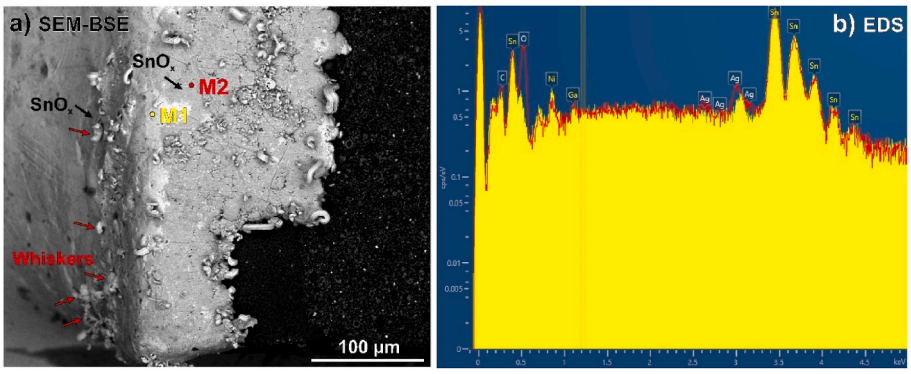

Fig. 4. Corrosion and whiskers on the lower meniscus of a SAC0307-0.5TiO_2 solder joint after 4000 h, 85C/85RH% TH test: a SEM-BSE micrograph; b) EDS spectra of the measurement points M1-M2.

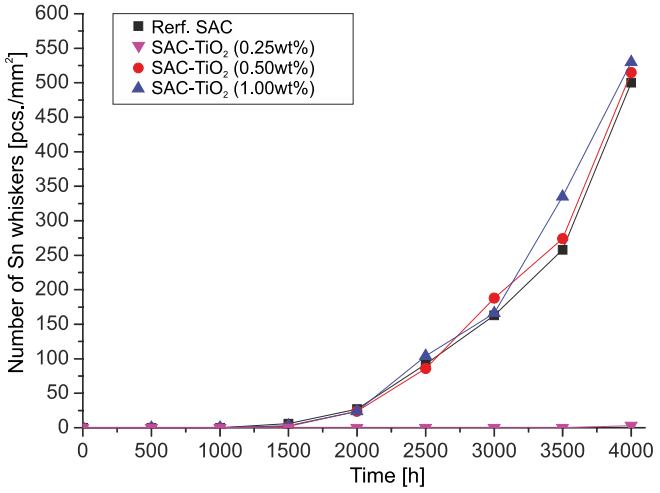

Fig. 5. Number of the detected whiskers during the 85C/85RH% TH test.

longest Sn whisker, which was to be found, was 47 µm on a SAC0307-1TiO_2 sample. Probably the intensive oxidation of the TH test, which also affected the surface of the whiskers, limited the length increase. No considerable difference has been found in the whisker susceptibility of ref. SAC0307 and higher TiO_2 content (0.5 and 1 wt%) solder alloys.

The SAC0307–0.25TiO_2 samples produced the first Sn whiskers only after 3500 h 85C/85RH% TH test, and only 3pcs per 1 mm^2 were found. Their lengths were between 6 and 10 µm. The main finding of the 4000 h TH test was that the ref. SAC0307 and the higher TiO_2 (0.5 and 1 wt%) content solder joints behaved very similarly; large corroded areas were developed on them with a lot of nodule-type Sn whiskers. Oppositely, the solder joint with a lower TiO_2 weight fraction (SAC0307–0.25TiO_2) showed a highly improved corrosion resistance and whiskering susceptibility.

4. Discussions

In order to study the observed correlation between the corrosion and the whisker growth, surface cuts were prepared at the whisker roots by FIB. Fig. 6 presents the microstructural analysis results of a nodule whisker (grew on a ref. SAC0307 sample) and the corroded area around them. The dimensions of the whisker were approximately 15–20 µm length, with 4–5 µm diameter (Fig. 6a). The FIB cut was performed Ga ion beam. Fig. 6b shows a SEM-BSE micrograph of the whisker root. The considerable contrast differences of the Sn grans at the whisker root suggested material differences that were approved EDS measurements (Fig. 6c). The right darker gray grains (M4 measurement point) were highly corroded (the peak of oxygen is considerable in the spectra); in contrast, the left light gray grains (M1 measurement point) were mostly pure Sn. A red dashed line in Fig. 6b marks the border between corroded and non-corroded Sn grains under the whisker (Fig. 6b).

These results suggested that there is a direct relation between corrosion and whisker growth. Corroded grains could initiate the Sn whisker growth, while the non-corroded grains supplied the Sn atoms to build the whisker body. The FIB cut revealed a contrast difference between the surface and the body of the whisker. This proved that the corrosion occurred on the surface of the whiskers too (M3 measurement point). This could be indirect evidence that the corrosion of the whiskers could limit their growth during the TH test. Sn can have two oxides: SnO and SnO_2, and two hydroxides: $Sn(OH)_2$ and $Sn(OH)_4$. All of them have negative Gibbs free energy and reduction potentials [26]. A chemical process occurs spontaneously (without external energy) when it's Gibbs free energy (ΔG^0) is negative; furthermore, each chemical compounds proceed to have a lower electrochemical potential.

Therefore, all Sn oxides and hydroxides can form in our system. At room conditions, Sn produces only a thin (in the nm range) oxide layer. However, in a wet environment, an electrochemical cell forms on the SnAgCu solder joint, which means that an anode and a cathode can be distinguished. This is caused by the heterogeneities in the component materials (like in our case, the Sn matrix contains different IMCs), and by the exposure circumstances (absorbed/condensed water film always contains Cl, S, Na, etc. contaminants which result in electrolyte formation).

The standard reduction potential of the possible IMCs in our system (Cu_6Sn_5, Cu_3Sn, and Ag_3Sn) is higher than this parameter of Sn [27], so the IMCs are cathodic to Sn. It resulted in Sn grains was corroding while the cathodic current protected the IMCs. The dissolution and corrosion occurred at the Sn grains, while the oxygen depolarization happened on the cathode. When Sn^{2+}/Sn^{4+} ions met with the OH^- ions, corrosion products formed at the cathode, and precipitates appeared. (Related chemical equations can be found in Ref. [27]).

The corrosion process of the SnAgCu solders could be accelerated towards the solder bulk [28], resulting in so-called localized corrosion, which caused the growth of a locally thick Sn-oxides layer (as we observed in Fig. 6). This process is illustrated in the case of the ref. SAC0307 samples in Fig. 7.

The development of the corrosion spots resulted in a volumetric expansion in the solder layer (marked by the red dashed lines) since the specific density of the Sn (7.31 g/cm^3) is higher than this parameter of the oxides (SnO 6.45 g/cm^3 and SnO_2 6.95 g/cm^3). The volumetric expansion of corroding Sn grains resulted in considerable mechanical stress on the neighboring ones (Fig. 7). These Sn grains relaxed the awakening stress by Sn whisker development. This explains that the whiskers were located close to corroded areas (as it was visible in Figs. 2 and 3).

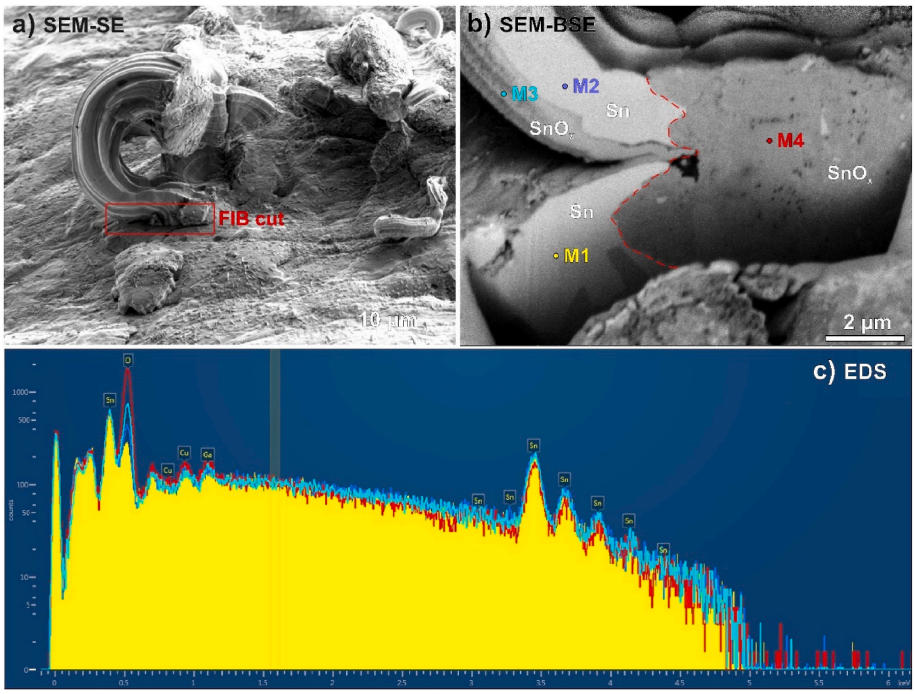

Fig. 6. Sn whisker on a SAC0307-0.5TiO_2 sample: a) The prepared whisker; b) SEM-BSE micrograph of the whisker root; c) EDS spectra of the measurement points M1-M4.

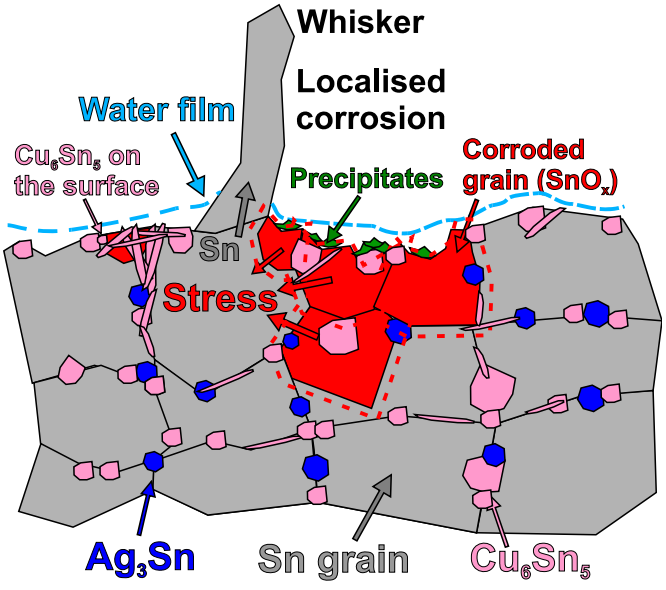

Fig. 7. Corrosion and whisker growth on a ref. SAC0307 sample.

In order to understand the role of the TiO_2 NPs in the corrosion process of the SnAgCu solder alloy, their incorporation mechanism needs to be investigated. One of the main effects of the ceramic NPs in the solder bulk is that they refine the microstructure of the solder joints, mainly the Sn grains, which can be refined even with an order of magnitude [13,14,29]. Metallographic cross-sections have been prepared from the solder joints to study their grain structure. Fig. 8 presents SEM-BSE micrographs of the solder bulk close to the Cu pad (Fig. 1). As it was expected, considerable refinement of the Sn grains has happened in the composite solder joints. The Sn grain boundaries are marked by red dashed lines according to the IMC network in the Sn matrix. The average Sn grain size was ~15 µm in the reference SAC0307 solder joints (Fig. 8a), which decreased to ~3 µm on average in the composite ones (Fig. 8c and d).

Generally, the smaller grains are not favorable from the point of corrosion. The corrosion process usually starts at the grain boundaries since it is more intense at places having higher surface free energy [30,31]. The grain structure refinement results in an extensive grain boundary network, which means high grain-boundary free energy of the system [32]. So the composite solder alloys suppose to show an accelerated corrosion behaviour compared to the reference SnAgCu. However, we found oppositely, in the case of higher weight fractions of TiO_2 (0.5 and 1 wt%) the corrosion resistance did not change significantly; furthermore, in the case of lower weight fractions of TiO_2 (0.25 wt%) the corrosion resistance improved considerably compared to the ref. SAC0307 solder alloy.

Therefore, the incorporation of the TiO_2 NPs into the Sn-matrix could explain the differing corrosion behaviour of composite solder alloys. Lala et al. [33] improved the corrosion properties of Sn layers with the addition of 1.3 wt% Cr, as was shown by the reduced corrosion current density by 40%. The Cr behaves very similarly in the Sn-matrix as the TiO_2 NPs do. Cr is hardly soluble in Sn [34], so it incorporates into the boundary of the Sn grains, and they cause refinement of the grains with the increase of high-angle grain boundaries. This helps the Cr particles to segregate between the Sn grains and to decrease the strain in the grains [33]. Under corrosive conditions, the homogeneously incorporated Cr can form a protective Cr-oxide layer between the Sn grains, acting as a corrosion protection layer. The TiO_2 NPs might have a similar effect but on a slightly different mechanism of action; furthermore, it also depends on the weight fraction of the TiO_2 NPs.

Fig. 9 presents the typical incorporation structures of the TiO_2 at the Sn grain boundaries by FE-SEM, STEM, and EDS techniques in the SAC0307–0.25TiO_2 and SAC0307-1TiO_2 solder joints. In the case of lower TiO_2 weight fraction (Fig. 9a), a more layer-like incorporation of the NPs is visible. It is nicely visible in the magnified STEM picture (Fig. 9b). The STEM-EDS allowed measurements with very fine spot size, so the presence of TiO_2 in the EDS spectrum was significant (Fig. 9c). In the case of a higher TiO_2 weight fraction (Fig. 9d), TiO_2 agglomerates were usually formed at the grain boundaries. Their sizes could reach

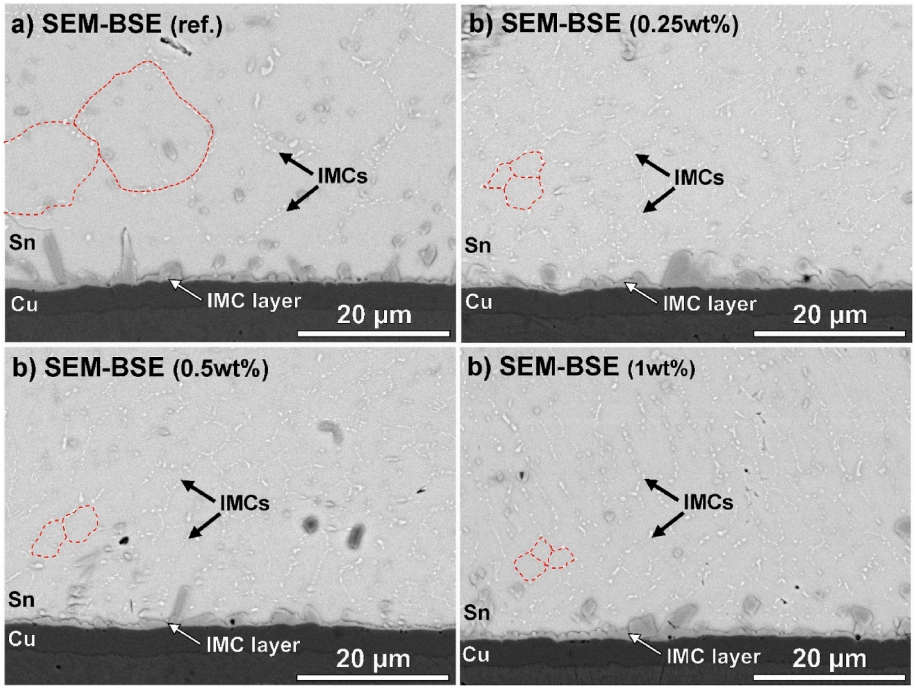

Fig. 8. Grain structure of the solder joints: a) ref SAC0307; b SAC-0.25TiO_2; c) SAC-0.5TiO_2; d) SAC-1TiO_2.

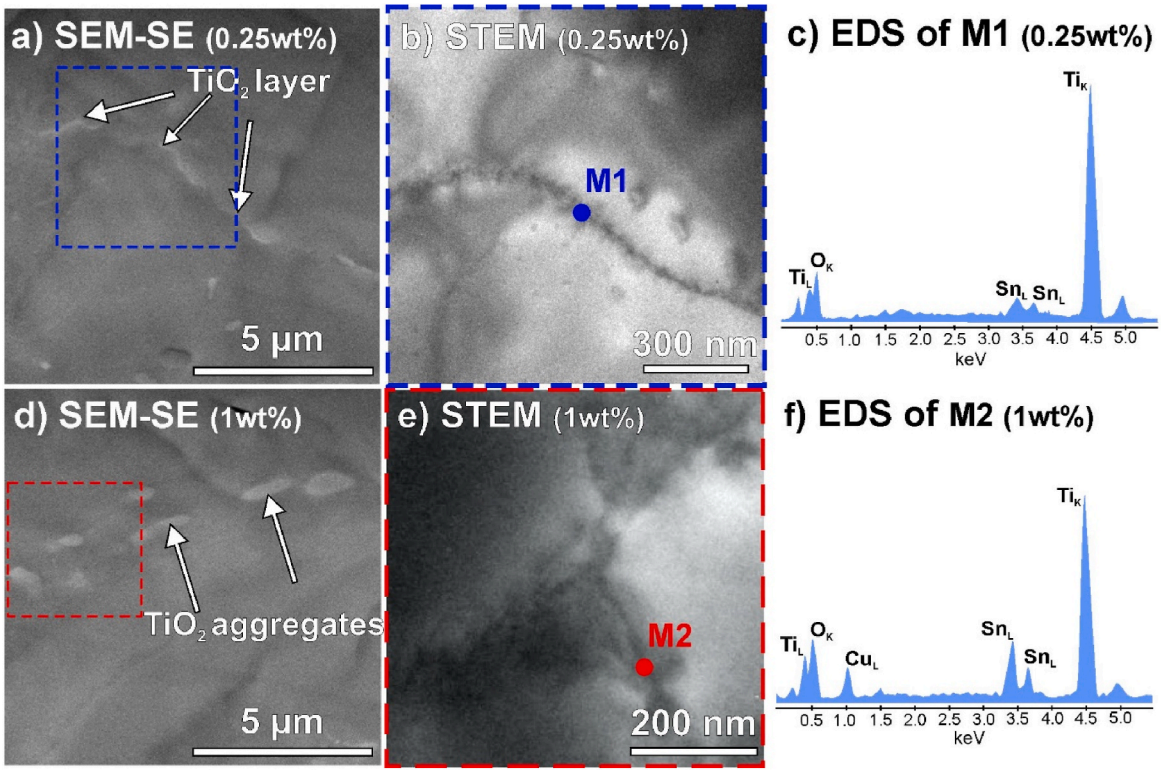

Fig. 9. Incorporation structure of the TiO_2: a) SEM - SE micrograph of SAC0307–0.25TiO_2; STEM investigation of the marked area in a); c) EDS spectrum of measurement point M1; d) SEM - SE micrograph of SAC0307-1TiO_2; e) STEM investigation of the marked area on d; f) EDS spectrum of measurement point M2.

even 1 μm (Fig. 9d), which means they contain hundreds of NPs. In this case, the STEM picture (Fig. 9e) is less informative; however, the EDS spectrum shows a large amount of TiO_2 (Fig. 9f). As previously reported, agglomeration of the NPs usually occurs at a higher weight fraction of the NPs [6,17,35].

The further question is whether the TiO_2 can have any reaction with the Sn. Beniwal et al. [36] growth successfully SnO_x clusters on the cleaned/activated surface of TiO_2 (110) rutile. They found that two Sn atoms in a cluster can incorporate an O from the TiO_2 surface to form Sn_2O. In our case, the key point is the flux in the solder paste. The flux is composed of a carrier/base and an active component which is usually some organic acid, like lactic, acetic, and oxalic [37–40]. They belong to

the family of carboxylic acids, which means that they contain a carboxyl group attached to an R-group like R–COOH. Carboxylic acids react with TiO_2 NPs at elevated temperatures (over 100 °C), like the soldering temperature, which can even leave hydroxyl (OH) groups on the TiO_2 surface [41].

The possible interaction between the TiO_2 and the Sn atoms was studied by density functional theory (DFT) calculations using plane-wave/pseudopotential formalism [42,43]. The calculations were carried out in the Quantum ESPRESSO software using the Perdew-Burke-Ernzerhof exchange-correlation functional. Wave functions have been expanded in plan waves up to a kinetic energy of 47.1 Ry, along with a cutoff of 424 Ry for the augmented density. The surface of TiO_2 rutile (110), as the most stable crystal face, was chosen to be the simulation surface, and the bonding of a single Sn atom was investigated. Two different surface conditions were examined to calculate the Sn atom absorption energy on TiO_2 surface. The first case was when an Sn atom would adsorb directly on TiO_2 surface oxide (Fig. 10a), and the second case was when an Sn atom would adsorb on TiO_2 surface hydroxyl group (Fig. 10c). The Sn atom was always located over the bulk [41,44].

The binding energy between TiO_2 and a single Sn atom is calculated as follows:

$$E_B = E_{sum} - E_{TiO_2} - E_{Sn} \tag{8}$$

where E_B is the binding energy between TiO_2 and Sn atom, E_{sum} is the sum system energy, E_{TiO2} is the energy of TiO_2 without the Sn atom, and E_{sn} is the energy of a single Sn atom. According to the DFT calculations, in the first case (Fig. 10a) the Sn atom oxidizes and absorbs on the TiO_2 surface (Fig. 10b) with a binding energy of 2.12 eV. In the second case, when the Sn atom is on TiO_2 hydroxyl group (Fig. 10c), it reduces an H atom and dissociates (Fig. 10d). Accordingly, it is supposed that in soldering conditions, the Sn atoms of the solder alloy could bond to the TiO_2 NPs through the O atoms of TiO_2.

The bonded TiO_2–Sn structure is not able to oxidize further. Therefore our assumption (Fig. 11), when the TiO_2 NPs are evenly (layer-like) distributed between the Sn grains, like in the case of low TiO_2 weight fraction, 0.25 wt%, they could increase the resistance of the composite solder alloys against corrosion, similarly, as Lala et al. [33] found in Sn coatings with Cr addition. The localized corrosion might occur despite the protection TiO_2 NPs, but the growth of the corrosion spots is much slower than in the ref. SAC0307 solder alloy.

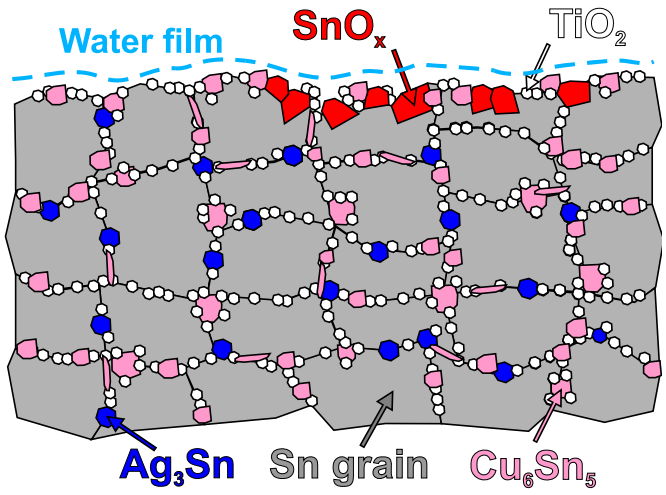

Fig. 11. Protective TiO_2–Sn oxide layer between the Sn grains in the SAC0307–0.25TiO_2 solder joints.

In the case of higher TiO_2 weight fractions (0.5 wt% and 1 wt%), TiO_2 NPs still refined the Sn grains, and they were located between the Sn grains, but their distribution differed from the lower weight fraction case (0.25 wt%), as it is illustrated in Fig. 12. TiO_2 agglomerates were formed at the grain boundaries, which could not perform such a corrosion protection effect as the layer-like incorporation in the case of the lower TiO_2 weight fraction (Fig. 11). So intensive localized corrosion occurred on the surface of the composite solder joints with 0.5/1 wt% of TiO_2 NPs (Fig. 12) like on the ref. SAC0307 samples (Fig. 7). Therefore,

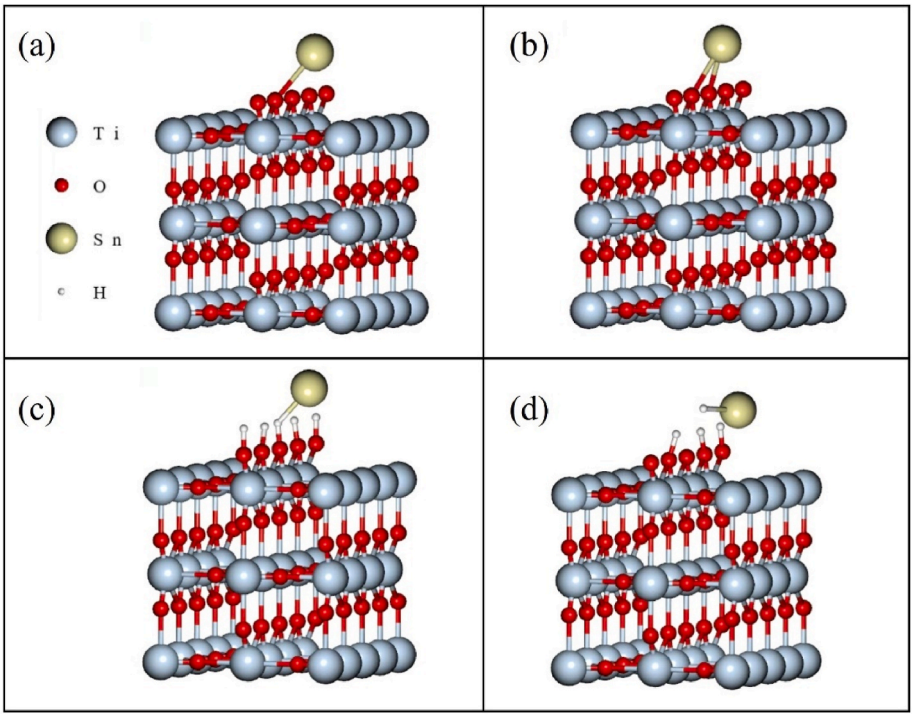

Fig. 10. DFT calculations: a) initial position of the Sn atom on TiO_2 surface; b) calculation results of the Sn atom on TiO_2 surface; c) initial position of the Sn atom on TiO_2 hydroxyl group; d) calculation results of the Sn atom on TiO_2 hydroxyl group.

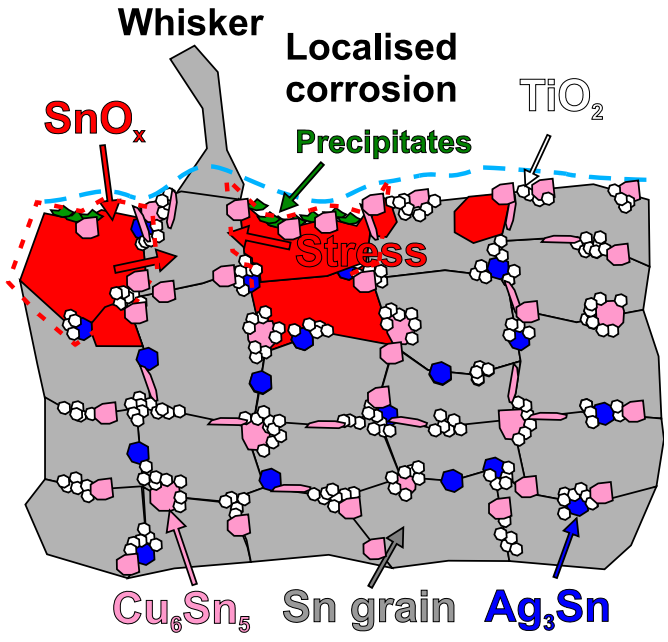

Fig. 12. Corrosion and whisker growth on the samples having higher TiO_2 weight fractions (0.5 and 1 wt%).

the composite solder joints with higher TiO_2 weight fractions (0.5 and 1 wt%) could produce Sn whiskers in the same way and in the same amounts as the ref. SAC0307.

Consequently, the weight fraction of the TiO_2 reinforcing NPs has been found crucial from the point of the reliability of the composite solder alloys. TiO_2 NPs in 0.25 wt% considerably improved the corrosion behavior of the composite solder joints and, as a consequence, inhibited the Sn whiskers under a corrosive environment. In the case of higher weight fractions (0.5 and 1 wt%) the TiO_2 NPs were prone to agglomerate, which limited their corrosion protection effect. Furthermore, the agglomerated NPs could deteriorate the structural integrity of the Sn-matrix [45,46]. Nevertheless, the composite solder joints with higher TiO_2 weight fractions were not more prone to whisker growth than the ref. SAC0307 solder joints.

5. Conclusion

The incorporation mechanism of TiO_2 NPs into SAC0307 solder alloy and their effect on the corrosion behavior of the composite solder alloys were investigated under corrosive conditions (85 °C/85RH%) and in the function of the weight fraction of the NPs. The solder joints suffered considerable corrosion and produced numerous Sn whiskers, except the composite solder joints with 0.25 wt% TiO_2 NPs. The microstructural analysis showed corroded Sn grains next to the whisker roots. Formation of SnO or SnO_2 resulted in a volumetric increase in the Sn layer since their density is lower than the Sn. This caused large mechanical stress on the neighboring not-corroded Sn grains. The mechanical stress was relaxed by whisker development.

The non-soluble TiO_2 NPs refined the Sn-matrix and segregated to the grain boundaries. However, differences were found in their distribution in the function of the weight fraction. TiO_2 NPs were incorporated layer-like in the case of lower weight fraction (0.25 wt%). While in the case of higher TiO_2 weight fractions, TiO_2 agglomerates were formed. DFT calculations proved that in soldering conditions, the Sn atoms of the solder alloy could bond to the TiO_2 NPs through the O atoms of TiO_2. The bonded TiO_2–Sn structure is not able to oxidize further. So the layer-like incorporation of the TiO_2 NPs (at 0.25 wt%) could slow down corrosion and suppress Sn whisker growth. The TiO_2 agglomerates (at 0.5 and 1 wt%) could not perform corrosion protection and whisker mitigation effects. Therefore, applying TiO_2 reinforcing NPs is suggested only in lower weight fractions (below 0.5 wt%) to improve the reliability parameters of SnAgCu solder alloys.

Data availability statement

The raw/processed data required to reproduce these findings cannot be shared at this time as the data also forms part of an ongoing study.

Declaration of competing interest

The authors declare that they have no known competing financial interests or personal relationships that could have appeared to influence the work reported in this paper.

Acknowledgement

This work was partially supported by the National Research Development and Innovation Office - Hungary (NKFIH), project FK127970, and by the NRDI Fund based on the charter of bolster issued by the NRDI Office under the auspices of the Ministry for Innovation and Technology.

References

[1] C. Xiong, Y. Xiao, J. Zhang, D. Luo, R. Goodall, Microstructure transformation and mechanical properties of Al alloy joints soldered with Ni-Cu foam/Sn-3.0Ag-0.5Cu (SAC305) composite solder, J. Alloys Compd. 922 (2022), 166135, https://doi.org/10.1016/j.jallcom.2022.166135.

[2] O. Krammer, T. Garami, B. Horvath, T. Hurtony, B. Medgyes, L. Jakab, Investigating the thermomechanical properties and intermetallic layer formation of Bi micro-alloyed low-Ag content solders, J. Alloys Compd. 634 (2015) 156–162, https://doi.org/10.1016/j.jallcom.2015.02.092.

[3] K.-S. Kim, S.-S. Kim, Y. Yorikado, K. Suganuma, M. Tsujimoto, I. Yanada, Sn whisker growth on Sn plating with or without surface treatment during the room temperature exposure, J. Alloys Compd. 558 (2013) 125–130.

[4] M.A. Ashworth, G.D. Wilcox, R.L. Higginson, R.J. Heath, C. Liu, R.J. Mo, The effect of electroplating parameters and substrate material on tin whisker formation, Microelectron. Reliab. 55 (2015) 180–191, https://doi.org/10.1016/j.microrel.2014.10.005.

[5] A.A. El-Daly, A. Fawzy, S.F. Mansour, M.J. Younis, Thermal analysis and mechanical properties of Sn–1.0 Ag–0.5 Cu solder alloy after modification with SiC nano-sized particles, J. Mater. Sci. Mater. Electron. 24 (2013) 2976–2988, https://doi.org/10.1007/s10854-013-1200-8.

[6] M.M. Salleh, S. McDonald, K. Nogita, Effects of Ni and TiO_2 additions in as-reflowed and annealed Sn0.7Cu solders on Cu substrates, J. Mater. Process. Technol. 242 (2017) 235–245, https://doi.org/10.1016/j.jmatprotec.2016.11.031.

[7] F.C. Ani, A. Jalar, A.A. Saad, C.Y. Khor, R. Ismail, Z. Bachok, M.A. Abas, N. K. Othman, SAC–xTiO_2 nano-reinforced lead-free solder joint characterizations in ultra-fine package assembly, Solder. Surf. Mt. Technol. 30 (2018) 1–13, https://doi.org/10.1108/SSMT-04-2017-0011.

[8] A.K. Gain, Y. Chan, W.K. Yung, Effect of additions of ZrO_2 nano-particles on the microstructure and shear strength of Sn–Ag–Cu solder on Au/Ni metallized Cu pads, Microelectron. Reliab. 51 (2011) 2306–2313, https://doi.org/10.1016/j.microrel.2011.03.042.

[9] A.K. Gain, L. Zhang, Microstructure, mechanical and electrical performances of zirconia nanoparticles-doped tin-silver-copper solder alloys, J. Mater. Sci. Mater. Electron. 27 (2016) 7524–7533, https://doi.org/10.1007/s10854-016-4732-x.

[10] L. Tsao, S. Chang, Effects of Nano-TiO_2 additions on thermal analysis, microstructure and tensile properties of Sn3.5Ag0.25Cu solder, Mater. Des. 31 (2010) 990–993, https://doi.org/10.1016/j.matdes.2009.08.008.

[11] D. Lin, S. Liu, T. Guo, G.X. Wang, T. Srivatsan, M. Petraroli, An investigation of nanoparticles addition on solidification kinetics and microstructure development of tin–lead solder, Mater. Sci. Eng. 360 (2003) 285–292, https://doi.org/10.1016/S0921-5093(03)00466-0.

[12] E.A. Eid, A.N. Fouda, E.S.M. Duraia, Effect of adding 0.5 wt% ZnO nanoparticles, temperature and strain rate on tensile properties of Sn–5.0 wt% Sb–0.5 wt% Cu (SSC505) lead free solder alloy, Mater. Sci. Eng. 657 (2016) 104–114, https://doi.org/10.1016/j.msea.2016.01.081.

[13] A. Skwarek, O. Krammer, T. Hurtony, P. Ptak, K. Górecki, S. Wroński, D. Straubinger, K. Witek, B. Illés, Application of ZnO nanoparticles in Sn99Ag0.3Cu0.7 based composite solder alloys, Nanomaterials 11 (2021) 1545, https://doi.org/10.3390/nano11061545.

[14] Y. Shi, J. Liu, Z. Xia, Y. Lei, F. Guo, X. Li, Creep property of composite solders reinforced by nano-sized particles, J. Mater. Sci. Mater. Electron. 19 (2007) 349–356, https://doi.org/10.1007/s10854-007-9327-0.

[15] M.A.A.M. Salleh, A.M.M. Al Bakri, H. Kamarudin, M. Bnhussain, F. Somidin, Solderability of Sn-0.7Cu/Si_3N_4 lead-free composite solder on Cu-substrate, Phys. Procedia 22 (2011) 299–304, https://doi.org/10.1016/j.phpro.2011.11.047.

[16] A. Fawzy, S. Fayek, M. Sobhy, E. Nassr, M. Mousa, G. Saad, Tensile creep characteristics of Sn–3.5Ag–0.5Cu (SAC355) solder reinforced with nano-metric ZnO particles, Mater. Sci. Eng. 603 (2014) 1–10, https://doi.org/10.1016/j.msea.2014.02.061.
[17] M. Ramli, N. Saud, M.M. Salleh, M.N. Derman, R.M. Said, M.I. Izwan, Effect of TiO_2 additions on Sn-0.7Cu-0.05Ni lead-free composite solder, Microelectron. Reliab. 65 (2016) 255–264, https://doi.org/10.1016/j.microrel.2016.08.011.
[18] G. Chen, L. Liu, V.V. Silberschmidt, Y. Chan, C. Liu, F. Wu, Retained ratio of reinforcement in SAC305 composite solder joints: effect of reinforcement type, processing and reflow cycle, Solder, Surf. Mt. Technol. 28 (2016) 159–166, https://doi.org/10.1108/SSMT-02-2016-0004.
[19] S.Y. Chang, C.C. Jain, T.H. Chuang, L.P. Feng, L.C. Tsao, Effect of addition of TiO_2 nanoparticles on the microstructure, microhardness and interfacial reactions of Sn3.5AgXCu solder, Mater. Des. 32 (2011) 4720–4727, https://doi.org/10.1016/j.matdes.2011.06.044.
[20] Y. Tang, Y.C. Pan, G.Y. Li, Influence of TiO_2 nanoparticles on thermal property, wettability and interfacial reaction in Sn–3.0Ag–0.5Cu–xTiO2 composite solder, J. Mater. Sci. Mater. Electron. 24 (2013) 1587–1594, https://doi.org/10.1007/s10854-012-0980-6.
[21] Y. Tang, G. Li, Y. Pan, Effects of TiO_2 nanoparticles addition on microstructure, microhardness and tensile properties of Sn–3.0Ag–0.5Cu–xTiO2 composite solder, Mater. Des. 55 (2014) 574–582, https://doi.org/10.1016/j.matdes.2013.10.033.
[22] S.S.M. Nasir, M.Z. Yahay, A.M. Erer, B. Illés, A.A. Mohamad, Effect of TiO_2 nanoparticles on the horizontal hardness properties of Sn-3.0Ag-0.5Cu-1.0TiO2 composite solder, Ceram. Int. 45 (2019) 18563–18571, https://doi.org/10.1016/j.ceramint.2019.06.079.
[23] A. Skwarek, P. Ptak, K. Górecki, T. Hurtony, B. Illés, Microstructure influence of SACX0307-TiO_2 composite solder joints on thermal properties o power LED assemblies, Materials 13 (2020) 1563, https://doi.org/10.3390/ma13071563.
[24] B. Illés, B. Horváth, Tin whisker growth from micro-alloyed SAC solders in corrosive climate, J. Alloys Compd. 616 (2014) 116–121, https://doi.org/10.1016/j.jallcom.2014.07.103.
[25] B. Illés, T. Hurtony, B. Medgyes, Effect of current load on corrosion induced tin whisker growth from SnAgCu solder alloys, Corrosion Sci. 99 (2015) 313–319, https://doi.org/10.1016/j.corsci.2015.07.026.
[26] S. Cho, J. Yu, S.K. Kang, D.-Y. Shih, Oxidation study of pure tin and its alloys via electrochemical reduction analysis, J. Electron. Mater. 34 (2005) 635–642, https://doi.org/10.1007/s11664-005-0077-6.
[27] P. Yi, C. Dong, K. Xiao, X. Li, Study on corrosion behavior of β-Sn and intermetallic compounds phases in SAC305 alloy by in-situ EC-AFM and first-principles calculation, Corrosion Sci. 181 (2021), 109244, https://doi.org/10.1016/j.corsci.2021.109244.
[28] B. Horváth, T. Shinohara, B. Illés, Corrosion properties of tin-copper alloy coatings in aspect of tin whisker growth, J. Alloys Compd. 577 (2013) 439–444, https://doi.org/10.1016/j.jallcom.2013.06.092.
[29] A. El-Daly, G. Al-Ganainy, A. Fawzy, M. Younis, Structural characterization and creep resistance of nano-silicon carbide reinforced Sn–1.0Ag–0.5Cu lead-free solder alloy, Mater. Des. 55 (2014) 837–845, https://doi.org/10.1016/j.matdes.2013.10.043.
[30] A. Gupta, C. Srivastava, Low-temperature Sn electrodeposition: texture evolution, grain boundary constitution and corrosion behavior, Surf. Coating. Technol. 425 (2021), 127709, https://doi.org/10.1016/j.surfcoat.2021.127709.
[31] A. Gupta, C. Srivastava, Temperature driven texture and grain boundary engineering of electrodeposited β-Sn coatings and its effect on the coating corrosion behaviour: five-parameter grain boundary character distribution analysis study, Scripta Mater. 196 (2021), 113763, https://doi.org/10.1016/j.scriptamat.2021.113763.
[32] K. Tsuji, Roll of grain-boundary free energy & surface free energy for tin whisker growth, in: Proc. Of the IPC/JEDEC 4th Intl. Conf. on Lead-Free Electronic Components and Assemblies, 2003.
[33] S.R.F. Lala, K.S. Jyotheender, A. Gupta, S. Arora, P. Kumar, C. Srivastava, Evolution of texture and strain in Sn coating with Cr addition and its effect on the coating corrosion behavior, Materialia 14 (2020), 100944, https://doi.org/10.1016/j.mtla.2020.100944.
[34] R. Rashidi, H. Naffakh-Moosavy, Metallurgical, physical, mechanical and oxidation behavior of lead-free chromium dissolved Sn–Cu–Bi solders, J. Mater. Res. Technol. 13 (2021) 1805–1825, https://doi.org/10.1016/j.jmrt.2021.05.055.
[35] H. Peng, G. Chen, L. Mo, Y.C. Chan, F. Wu, H. Liu, An investigation on the ZnO retained ratio, microstructural evolution, and mechanical properties of ZnO doped Sn3.0Ag0.5Cu composite solder joints, J. Mater. Sci. Mater. Electron. 27 (2016) 9083–9093, https://doi.org/10.1007/s10854-016-4943-1.
[36] S. Beniwal, W. Chai, K. Metavarayuth, T.D. Maddumapatabandi, D.M. Shakya, G. Henkelman, D.A. Chen, Oxidation of Sn at the Cluster−Support interface: Sn and Pt−Sn clusters on TiO_2(110), J. Phys. Chem. C 125 (2021) 17671–17683, https://doi.org/10.1021/acs.jpcc.1c03338.
[37] R. Datta, M. Henry, Lactic acid: recent advances in products, processes and technologies – a review, J. Appl. Chem. Biotechnol. 81 (2006) 1119–1129, https://doi.org/10.1002/jctb.1486.
[38] J. Vijayakumar, R. Aravindan, T. Viruthagiric, Recent trends in the production, purification and application of lactic acid, Chem. Biochem. Eng. Q. 22 (2008) 245–264.
[39] M. Nasta, H.C. Peebles, A model of the solder flux reaction; reactions at the metal/metal oxide/electrolyte solution interface, Circ. World 21 (1995) 10–13, https://doi.org/10.1108/eb044043.
[40] S. Kwon, W. Seo, K. Wonil, Y.H. Ko, H.J. Lee, S. Yoo, Effects of flux activator on wettability and slump of Sn-Ag-Cu solder paste, J. Microelectron. Packag. Soc. 25 (2018) 123–128, https://doi.org/10.6117/kmeps.2018.25.4.123.
[41] Q. Qu, H. Geng, R. Peng, Q. Cui, X. Gu, F. Li, M. Wang, Chemically binding carboxylic acids onto TiO_2 nanoparticles with adjustable coverage by solvothermal strategy, Langmuir 26 (2010) 9539–9546, https://doi.org/10.1021/la100121n.
[42] F. Mondaca, F.A. Calderón, S. Conejeros, A.I. Mtz-Enriquez, The optoelectronic properties of Eu/F-codoped tin oxide, an experimental and DFT study, Ceram. Int. 47 (2021) 31756–31764, https://doi.org/10.1016/j.ceramint.2021.08.057.
[43] T. Jan, S. Azmat, A.U. Rahman, S.Z. Ilyas, A. Mehmood, Experimental and DFT study of Al doped ZnO nanoparticles with enhanced antibacterial activity, Ceram. Int. 48 (2022) 20838–20847, https://doi.org/10.1016/j.ceramint.2022.04.073.
[44] J. Balajka, U. Aschauer, S.F.L. Mertens, A. Selloni, M. Schmid, U. Diebold, Surface structure of TiO2 rutile (011) exposed to liquid water, J. Phys. Chem. C 121 (2017) 26424–26431, https://doi.org/10.1021/acs.jpcc.7b09674.
[45] M. Peron, R. Bertolini, S. Cogo, On the corrosion, stress corrosion and cytocompatibility performances of ALD TiO_2 and ZrO_2 coated magnesium alloys, J. Mechanical. Behav. Biomed. Mater. 125 (2022), 104945, https://doi.org/10.1016/j.jmbbm.2021.104945.
[46] L.X. Ying, K. Wu, D.Y. Li, C.X. Wu, Z. Fu, TiO_2 Sol strengthened Cu-Sn-PTFE composite coatings with high homogeneity and superior resistance to wear, Wear 426–427 (2019) 258–264, https://doi.org/10.1016/j.wear.2019.01.031.